RSC Advances

This is an *Accepted Manuscript*, which has been through the Royal Society of Chemistry peer review process and has been accepted for publication.

Accepted Manuscripts are published online shortly after acceptance, before technical editing, formatting and proof reading. Using this free service, authors can make their results available to the community, in citable form, before we publish the edited article. This *Accepted Manuscript* will be replaced by the edited, formatted and paginated article as soon as this is available.

You can find more information about *Accepted Manuscripts* in the Information for Authors.

Please note that technical editing may introduce minor changes to the text and/or graphics, which may alter content. The journal's standard Terms & Conditions and the Ethical guidelines still apply. In no event shall the Royal Society of Chemistry be held responsible for any errors or omissions in this *Accepted Manuscript* or any consequences arising from the use of any information it contains.

ROYAL SOCIETY OF CHEMISTRY

www.rsc.org/advances

Application of $H_4SiMo_{12}O_{40}$@SiO_2 catalyst with hollow core-shell structure to oxidative desulfurization

Xiaotian Zhang [a], Guangqin Luo [a], Mingyuan Zhu [a, b,*], Lihua Kang [a, b], Feng Yu [a, b], Bin Dai [a, b]

a. School of Chemistry and Chemical Engineering of Shihezi University, Shihezi, Xinjiang 832000, P.R. China.

b. Key Laboratory for Green Processing of Chemical Engineering of Xinjiang Bingtuan, Shihezi, Xinjiang 832000, P.R. China.

* Corresponding Author Phone: +86 9932057270; Fax: +86 9932057210;

E-mail: zhuminyuan@shzu.edu.cn (Mingyuan Zhu);

RSC Advances Accepted Manuscript

Abstract

Designing a catalyst with excellent recyclability to improve oxidative desulfurization continues to challenge many researchers. In this study, $H_4SiMo_{12}O_{40}$@SiO_2 catalyst with a core-shell structure was successfully prepared and applied to desulfurize a model oil. Various characterization methods demonstrated that the synthesized $H_4SiMo_{12}O_{40}$@SiO_2 catalyst presents a hollow spherical structure and that the active $H_4SiMo_{12}O_{40}$ species is incorporated into the mesoporous SiO_2 shell. Under optimal reaction conditions, the desulfurization rate of dibenzothiophene is nearly 100%, and the activation energy of the oxidation reaction of dibenzothiophene is 22.08 kJ/mol. These results reveal the excellent catalytic activity of $H_4SiMo_{12}O_{40}$@SiO_2 for oxidative desulfurization. The catalyst can be recycled by up to 13 times without significant reductions in catalytic activity; such enhanced recyclability may be attributed to the core-shell structure of the synthesized catalyst.

Keywords: Core-shell structure; Oxidative desulfurization; Silicomolybdic acid; Recycling

RSC Advances Accepted Manuscript

1. Introduction

Ultra-deep desulfurization of fuels has recently attracted increased attention from the scientific community because of increasing environmental concerns and more stringent legal requirements.[1-3] So a great quantity of desulfurization methods have been researched. Xun et al. reported the catalytic oxidative desulfurization (ECODS) system was established by supported ionic liquid [Bmim]$FeCl_4$/Am TiO_2, which showed an outstanding catalytic performance with low amount of supported ionic liquid, the catalytic efficiency still remain 100% after recycling for 25 times.[4] Chen and co-workers prepared the peroxotungsten anions-based ionic liquid-type catalysts with H_2O_2 as oxidizing agent, the catalyst exerted remarkable desulfurization activity and recyclability under solvent-free and mild reaction conditions.[5] The desulfurization system with [Bmim]BF_4 was studied by Wang et al., the results indicated that the molecular oxygen can be applied as oxidant for oxidative desulfurization instead of H_2O_2.[6] Meanwhile, the ionic liquids also has been tried to apply for oxidative desulfurization, the oxidation desulfurization of fuel were carried out in Fenton-like ionic liquids/H_2O_2 system, the deep desulfurization can be accomplished in [Et_3NHCl] $FeCl_3$ for only 5 min at room temperature. EODS process was applied to prehydrotreated gasoline and the sulfur content can decline from 150 to 15 mg L^{-1} after two circulations of reaction.[7] The solid acidic ionic liquid polymer (PIL) was prepared and employed in investigating oxidation desulfurization. The oxidation activities were investigated using oxidizing benzothiophene, the results showed that the PIL was very efficient for oxidizing benzothiophene.[8] Among the various

RSC Advances Accepted Manuscript

desulfurization methods currently available, oxidative desulfurization (ODS) combined with extraction is considered an effective method for removing sulfur compounds from model oil because the process can be performed at low temperatures and atmospheric pressure.

H_2O_2 is commonly used as the oxidizing reagent during ODS, which may be catalyzed by formic acid，[9] acetic acid,[10] and heteropolyacids (HPA). García-Gutiérrez et al reported that Tungsten supported catalysts were synthesized for being applied in the oxidative desulfurization using H_2O_2 as an oxidant, $[H_2W_{12}O_{39}(O_2)]^{6-}$ and $[P_2W_{18}O_{61}(O_2)]^{6-}$ catalysts showed the decent activity with a sulfur elimination of 70.7%.[11] Moreover, $H_3PW_{12}O_{40}$ (HPW) and $H_3PMo_{12}O_{40}$ (HPMo) are promising catalysts for ODS in a liquid–liquid reaction system.[12, 13] In the presence of excess H_2O_2, the $W(O)_n$ complex in HPW can be peroxidized and disaggregated to form a peroxometal complex, such as $W(O_2)_n$, which improves catalytic activity during ODS.[14] However, as a homogeneous catalyst, HPA is difficult to separate from the ODS system, and its poor recyclability limits its industrial application. To overcome this problem and enhance its recyclability, researchers have adopted a solid support for HPA. Yan et al. synthesized HPW/SiO_2[15] and HPW/TiO_2[16] catalysts to increase the catalytic activity and recyclability of HPA during ODS. Zhang et al. applied a HPMo/SiO_2 catalyst for ODS and reported a conversion rate of nearly 100% for dibenzothiophene (DBT) in a model oil.[17] However, given the weak interaction between the active HPA and the solid support, HPA species easily dissolve in the water phase of the ODS system, which leads to the low recyclability of the catalyst. In

RSC Advances Accepted Manuscript

our previous work, we attempted to address this problem by functionalizing the solid support; thus, we used an amino group to improve electronic interactions between the anion of HPA and the amino cation. This method effectively improved the recyclability of HPA.[17, 18] However, HPA can still leach from the support after about six rounds of recycling because of the weak physical interaction between the active HPA species and the solid support. Thus, novel approaches to design the structure of the HPA catalyst remain necessary to prevent leaching of the HPA species and further enhance the recyclability of the catalyst during ODS.

According to the recent reports, the different ordered mesoporous silicas were synthesized and applied for investigation of oxidative desulfurization activities of dibenzothiophene and 4, 6-dimethyldibenzothiophene, the results demonstrated that oxidative desulfurization catalytic activities ascend with surface area and surface acidity of the mesoporous silicas.[19] Reference to above, in this work, we synthesized $H_4SiMo_{12}O_{40}@SiO_2$, which exhibits a core-shell structure, and applied this catalyst to the ODS of a model oil; mesoporous SiO_2 was used as the shell of the catalyst (Fig. 1). The reactants DBT and H_2O_2 were allowed to diffuse across the mesopores of the SiO_2 shell, after which the reaction system was catalyzed by $H_4SiMo_{12}O_{40}$ to produce sulfone. Given that the molecular size of $H_4SiMo_{12}O_{40}$ is larger than the pore size of SiO_2, leaching of the dissolved $H_4SiMo_{12}O_{40}$ into the ODS system is prevented, consequently improving the recyclability of the catalyst.

2. Experimental section

2.1. Materials

RSC Advances Accepted Manuscript

DBT (99%) used in the study was purchased from J&K Scientific Company. Th (99%), BT (97%) and 4,6-dimethyldibenzothiophene (4,6-DMDBT, 99%) were supplied by Aladdin. Ammonium molybdate (99%) was procured from Tianjin KaDa Chemical Co., Ltd. Cetyl trimethyl ammonium chloride, Triethanolamine, Ethyl orthosilicate was acquired from Tianjin GuangFu Chemical Co., Ltd. Ethanol absolute, Acetone, Methanol were purchased from Tianjin FuYu Chemical Co., Ltd. n-Octane was purchased from Sinopharm Chemical Reagent Co., Ltd. All reagents were used as received.

2.2. Catalyst preparation

The $H_4SiMo_{12}O_{40}@SiO_2$ catalyst was synthesized according to a previously reported method.[18] About 1.5 g of ammonium heptamolybdate was dissolved in a mixture of 220 mL of deionized water and 100 mL of ethanol. Polyvinyl-pyrrolidone (5 g) was then added to this mixture, and the solution was stirred for 30 min at room temperature. The resulting solution was placed in a Teflon-lined stainless steel autoclave and then hydrothermally treated in an oven at 453 K for 16 h. After cooling to room temperature, the products were centrifuged and washed four times with ethanol–acetone. The precipitates obtained from the reaction presented as MoO_2 nanoparticles. Exactly 10, 20, 30, or 40 mg of these nanoparticles was separately added to a mixture of 330 mL of deionized water and 200 mL of ethanol, and the resulting solution was ultrasonicated for 30 min. About 5.5 mL of 25% hexadecyltrimethylammonium chloride (CTACl) and 2 mL of triethanolamine were subsequently added to this mixture followed by thorough stirring for another 30 min

RSC Advances Accepted Manuscript

at room temperature. Exactly 4 mL of tetraethylorthosilicate was then added to the reaction system. The resulting mixture was stirred at room temperature for 16 h and centrifuged; the precipitates obtained were washed using ethanol–acetone and then dried overnight in an oven at 353 K. The obtained MoO_2@SiO_2 core-shell precursors were calcined in a muffle oven and subsequently exposed to air at 823 K for 6 h to remove the organic template. The resulting white products were labeled Mo^{VI}@SiO_2-X (X = 10, 20, 30, 40). $H_4SiMo_{12}O_{40}$@SiO_2 was prepared by immersion of the synthesized Mo^{VI}@SiO_2 (e.g., 0.1 g) into deionized water followed by centrifugation for 30 min and then air drying at 373 K for 4 h. After hydration, the color of the Mo^{VI}@SiO_2 changed from white to yellow-green. The synthesized catalyst was then labeled $H_4SiMo_{12}O_{40}$@SiO_2-X (X= 10, 20, 30, 40).

2.2. Material characterization

Transmission electron microscopy was performed using Tecnai F30 field emission transmission electron microscope. Bruno–Emmett–Teller (BET) surface area analysis was performed by using Micromeritics ASAP 2020 system to obtain the nitrogen adsorption isotherm at 77 K. All samples were degassed under vacuum at 383 K for 6 h. The average pore diameter and pore volume were calculated using the Barrett−Joyner−Halenda method. Powder X-ray diffraction (XRD) data were obtained using Bruker advanced D8 X-ray diffractometer operated at 40 kV and 40 mA with Cu-Kα irradiation (λ =1.5406 Å). FT-IR spectra were obtained using Nicolet AVATAR 360. Thermogravimetric analysis (TGA) was conducted using a TGA/DTA system (SDT Q600, America) with a nitrogen flow of 10 mL/min at room temperature up to

RSC Advances Accepted Manuscript

1173 K.

2.3. Catalytic ODS of the model oil

ODS experiments were performed in a 100 mL three-necked batch reactor. After heating 10 mL of the model oil with 100 ppm sulfur, thiophene (Th), benzothiophene (BT), dibenzothiophene (DBT), or 4,6-DMDBT was dissolved in *n*-octane to a desired temperature. The amounts of H_2O_2 and $H_4SiMo_{12}O_{40}@SiO_2$ catalyst in these mixtures were then optimized. The optimal $H_4SiMo_{12}O_{40}@SiO_2$ catalytic oxidation system included 27.2 μL of 30% H_2O_2 solution and 0.1g of the $H_4SiMo_{12}O_{40}@SiO_2$ catalyst. These components were subsequently mixed in a flask, and the mixture was magnetically stirred throughout the experiment by a reflux condenser to prevent solvent vaporization. The solution was periodically sampled for analysis, and the sulfur content of the clear model oil was analyzed using a microcoulometric detector (WK-2D) after the reaction. The catalysts were recycled via filtration and washed with methanol.

3. Results and discussion

3.1. Catalyst characterization

The average size of the MoO_2 nanoparticles is 43.55 nm (Fig. 2a). Fig. 2b shows the size distribution of MoO_2 nanoparticles. Under higher magnifications, in Fig.2c, the size of MoO_2 nanoparticles becomes more obvious. Fig. 2d shows that the MoO_2 nanoparticles were successfully coated with uniform silica shells and that CTACl was removed after heat treatment using hot air (823 K) for 6 h. Hollow cavities formed within the mesoporous spheres (Fig. 2e). After calcination, the overall size of the

RSC Advances Accepted Manuscript

silica spheres remained constant, thereby demonstrating the stability of the silica shells. The MoO_2 cores of $H_4SiMo_{12}O_{40}@SiO_2$ disappeared in nearly all of the spheres (Fig. 2f). These results demonstrate that silicomolybdic acid was successfully incorporated into the mesoporous silica hollow spheres.

Wide-angle XRD patterns revealed the absence of the characteristic peaks of the crystalline phase of molybdenum in the $H_4SiMo_{12}O_{40}@SiO_2$-X samples (Fig. 3a). The XRD patterns of all four $H_4SiMo_{12}O_{40}@SiO_2$-X samples showed a diffraction peak at $2\theta = 23.5°$, which suggests that the cell wall-free mesoporous silica is amorphous.[20, 21] However, $H_4SiMo_{12}O_{40}@SiO_2$-X (X = 10, 20, 30, and 40) showed no characteristic peaks of HSiMo, which demonstrates that HSiMo is highly dispersed on the surface of the SiO_2 support. Shown in Fig.3b, the crystalline phase of the oxide core nanoparticles can be assigned perfectly to monoclinic MoO_2 (JCPDS card no. 32-0671, space group: $P2_1 / n$, $a_o = 5.606$ Å, $b_o = 4.859$ Å, and $c_o = 5.537$ Å).

All of the mesoporous samples exhibited type IV isotherms (Fig. 4a), which may be attributed to their type H4 hysteresis loops.[22] As shown in Fig.4b, the average pore size is very uniform and centered at around 2.5 nm, based on a Micromeritics ASAP 2020 analysis with the data of adsorption branch. These values are slightly lower than those reported by Zeng et al (2.6 nm).[18] The decrease in the BET surface area (Table 1) and pore volume could be ascribed to the heteropolyanion-assisted attachment of the mesopores to the support. The S_{BET} of $H_4SiMo_{12}O_{40}@SiO_2$-X(X=10, 20, 30 and 40) are 802, 713, 653 and 440 m^2g^{-1}, respectively. This results were slightly higher than those reported by Zeng et al (701, 620, 445 and 156 m^2g^{-1})[18]. This result suggests that

RSC Advances Accepted Manuscript

the mesoporous structure of the SiO_2 support was preserved in all of the synthesized materials after loading of the $H_4SiMo_{12}O_{40}$ active species.

The peaks at 3451 and 1627 cm^{-1} can be assigned to the adsorption of water or surface OH groups, whereas the bands at 1250 to 1050, 802, and 470 cm^{-1} can be attributed to the silica matrix, as previously reported (Fig. 5).[23] These peaks respectively correspond to asymmetric stretching, symmetric stretching, and Si–O–Si bond bending vibrations.[24] Aside from the Si–O–Si band, which is characteristic of pure silica, a wide band at 956 cm^{-1} is observed in the spectra of hollow $H_4SiMo_{12}O_{40}$@SiO_2-X (X = 10, 20, 30, 40) spheres. This band is attributed to the surface of the terminal Mo=O vibration molybdic acid polymer phase. A weak peak at 910 cm^{-1} is ascribed to Mo−O−Si vibrations, which indicates a strong chemical interaction between the surface polymeric molybdate species and the mesoporous silica shells.[25] In addition, the FT-IR spectra revealed the Keggin structure of $H_4SiMo_{12}O_{40}$ in the $H_4SiMo_{12}O_{40}$@SiO_2-X catalysts.

3.2. Catalytic Reactivity

Fig. 6a shows that the sulfur removal rate tends to plateau when the O/S molar ratio reaches a value of 8; at this point, DBT is completely oxidized to $DBTO_2$.[26] This O/S value is only four times greater than the stoichiometric value (O/S = 2). The optimal O/S molar ratio is much greater than the stoichiometric ratio, which may be ascribed to the decomposition of H_2O_2 during ODS. This result demonstrates that an excess amount of oxidant improves DBT conversion, whereas the chemical reaction and the water produced from thermal decomposition hinder ODS.[27] In order to calculate the

RSC Advances Accepted Manuscript

selectivity of hydrogen peroxide in ODS process, we carried out the experiments to test the consumption of hydrogen peroxide in the reaction by titrating with mineral chameleon. The obtained conversion of H_2O_2 is about 97% after 1 h. Therefore, in order to achieve the optimal DBT conversion, the O/S molar ratio of 8:1 was selected as the optimal condition. The optimum dosage of the $H_4SiMo_{12}O_{40}$@SiO_2-20 catalyst was also determined during the conversion of DBT in 10 mL of a model oil containing 100 ppm of organic sulfur (Fig. 6b). The desulfurization rate of DBT conversion increased with increasing catalyst dosage, although no significant change in the desulfurization rate of DBT was observed when the catalyst dosage was increased from 0.08 g to 0.1 g. This result indicates that a catalyst dosage of 0.08 g is adequate to provide active sites for ODS. Moreover, increases in reaction temperature significantly increased the rate of $H_4SiMo_{12}O_{40}$@SiO_2-20 catalyzed desulfurization (Fig. 6c). When the reaction temperature was increased from 303 K to 343 K, the desulfurization rate significantly increased from 97% to 100%. Thus, when the temperature increases, the amount of $Mo(O_2)_n$ produced and the oxidation ability of DBT both increase. However, excessively high reaction temperatures can decompose H_2O_2 and reduced the amount of $Mo(O_2)_n$ produced. This result explains the desulfurization rate decreases at temperatures higher than 333 K.[28, 29] Therefore, the optimal temperature is 333 K for the $H_4SiMo_{12}O_{40}$@SiO_2-20 catalyst in the ODS process

Fig. 7 shows the following hierarchy of oxidation reactivity: DBT > 4,6-DMDBT > BT > Th. This pattern is affected by the varying electron density of the sulfur atom in

RSC Advances Accepted Manuscript

each of these compounds. The electron densities of sulfur atoms in 4,6-DMDBT, BT, Th, and DBT are 5.760, 5.739, 5.696, and 5.758, respectively.[30] The electron density of the sulfur atom in Th is smaller than that in DBT; thus, the catalytic activity of Th is lower than that of DBT. However, while the electron density of 4,6-DMDBT is higher than that of DBT, the oxidation reaction of the former is far lower than that of the latter. This observation may be attributed to the steric hindrance afforded by the methyl group, which inhibits the active species from interacting with the sulfur atom. Thus, the catalytic performances of these sulfur compounds are affected by both their electron density and steric hindrance.

We investigated the kinetics of DBT conversion at various temperatures by keeping the stirring speed fixed at 1000 rpm so that the mass transfer resistance is maintained at its minimum value. In the presence of excess H_2O_2, the oxidation of the sulfur components follows a pseudo-first order kinetics, as shown below.[31, 32]

$$r = -\frac{d_{C_t}}{dt} = k_{C_t} \qquad (1)$$

$$\ln(c_t / c_0) = -kt \qquad (2)$$

$$\ln k = \ln A - \frac{Ea}{RT} \qquad (3)$$

In the formula, k is the rate constant of the first-order kinetics reaction, and its value may be obtained from the plot of $\ln(c_0/c_t)$ as a function of reaction time. The reaction constant can be obtained from $\ln(c_0/c_t)$ at 303, 313, 323, and 333 K, wherein a linear relationship is observed (Fig. 8a). Based on the reaction rate constant k of the Arrhenius equation, we calculated the activation energy of DBT oxidation at various

RSC Advances Accepted Manuscript

temperatures by using Eq. (3). Fig. 8b shows that the activation energy of the oxidative desulfurization reaction is 22.08 kJ/mol. The activation energy of the $H_4SiMo_{12}O_{40}$@SiO_2-20 catalyst is lower than the reported value,[33] which demonstrates that the proposed catalyst has high activity.

At the end of the reaction, the catalyst was recovered via simple filtration, washed with methanol, dried, and then subjected to another cycle of ODS (Fig. 9). The desulfurization rate of the catalyst exceeded 90% even after 13 rounds of recycling. This result demonstrates that the mesoporous structure of the SiO_2 core can inhibit leaching of the active $H_4SiMo_{12}O_{40}$ species, thereby ensuring that the $H_4SiMo_{12}O_{40}$@SiO_2 catalyst possesses excellent recyclability.

As shown in Fig. 10, the fresh and used catalysts were characterized by IR spectroscopy. We found that the fresh catalyst $H_4SiMo_{12}O_{40}$@SiO_2-20 and after recovery of $H_4SiMo_{12}O_{40}$@SiO_2-20 have almost no change in peaks, it is demonstrated that the structure of catalyst $H_4SiMo_{12}O_{40}$@SiO_2-20 have an excellent stability.

4. Conclusions

In summary, we synthesized $H_4SiMo_{12}O_{40}$@SiO_2 with a core-shell structure and applied it to ODS. The as-synthesized catalysts exhibited excellent catalytic activity for the removal of sulfur compounds. The sulfur content in the model oil was reduced from 100 ppm to 0 ppm through methanol extraction for 90 min in the presence of an oxidant (O/S molar ratio = 8). The hierarchy of the catalytic activities of the different sulfur compounds showed the following order: DBT > 4,6-DMDBT > BT > Th. The

RSC Advances Accepted Manuscript

$H_4SiMo_{12}O_{40}@SiO_2$ catalyst could be recycled by up to 13 times without significant reductions in activity. Given its excellent recyclability, $H_4SiMo_{12}O_{40}@SiO_2$ is a promising catalyst for the industrial application of ODS.

Acknowledgments

This work was financially supported by young scientific and technological innovation leader of Bingtuan (2015BC001), Innovation project of graduate student in Xinjiang (XJGRI2015042), the Doctor Foundation of Bingtuan (No. 2013BB010), and the Foundation of Young Scientist in Shihezi University (No. 2013ZRKXJQ03).

References

1. E. Lorençon, D. C. Alves, K. Krambrock, E. S. Ávila, R. R. Resende, A. S. Ferlauto and R. M. Lago, *Fuel*, 2014, **132**, 53-61.
2. H. Song, J. Gao, X. Chen, J. He and C. Li, *Applied Catalysis A: General*, 2013, **456**, 67-74.
3. H. Wu, A. Duan, Z. Zhao, D. Qi, J. Li, B. Liu, G. Jiang, J. Liu, Y. Wei and X. Zhang, *Fuel*, 2014, **130**, 203-210.
4. S. Xun, W. Zhu, D. Zheng, H. Li, W. Jiang, M. Zhang, Y. Qin, Z. Zhao and H. Li, *RSC Advances*, 2015, **5**, 43528-43536.
5. J. Chen, C. Chen, R. Zhang, L. Guo, L. Hua, A. Chen, Y. Xiu, X. Liu and Z. Hou, *RSC Advances*, 2015, **5**, 25904-25910.
6. J. Wang, Q. Guo, C. Zhang and K. Li, *RSC Advances*, 2014, **4**, 59885-59889.
7. W. Zhu, J. Zhang, H. Li, Y. Chao, W. Jiang, S. Yin and H. Liu, *RSC Advances*, 2012, **2**, 658-664.

RSC Advances Accepted Manuscript

8. J. Wu, Y. Gao, W. Zhang, Y. Tan, A. Tang, Y. Men and B. Tang, *RSC Adv.*, 2014, **4**, 58800-58804.

9. P. S. Tam, J. R. Kittrell and J. W. Eldridge, *Industrial & Engineering Chemistry Research*, 1990, **29**, 321-324.

10. M. Te, C. Fairbridge and Z. Ring, *Applied Catalysis A: General*, 2001, **219**, 267-280.

11. J. L. García-Gutiérrez, G. C. Laredo, P. García-Gutiérrez and F. Jiménez-Cruz, *Fuel*, 2014, **138**, 118-125.

12. Y. Zhang, H. Lü, L. Wang, Y. Zhang, P. Liu, H. Han, Z. Jiang and C. Li, *Journal of Molecular Catalysis A: Chemical*, 2010, **332**, 59-64.

13. Y. ZHANG, W. Lu, Y. ZHANG, Z. JIANG and L. Can, *Chinese Journal of Catalysis*, 2011, **32**, 235-239.

14. T. Sachdeva and K. Pant, *Fuel Processing Technology*, 2010, **91**, 1133-1138.

15. X. M. Yan, J. H. Lei, D. Liu, Y. C. Wu and L. P. Guo, *Journal of the Chinese Chemical Society*, 2007, **54**, 911-916.

16. X.-M. Yan, P. Mei, J. Lei, Y. Mi, L. Xiong and L. Guo, *Journal of Molecular Catalysis A: Chemical*, 2009, **304**, 52-57.

17. M. Zhang, W. Zhu, S. Xun, J. Xiong, W. Ding, M. Li, Q. Wang and H. Li, *Chemical Engineering & Technology*, 2015, **38**, 117-124.

18. J. Dou and H. C. Zeng, *Journal of the American Chemical Society*, 2012, **134**, 16235-16246.

19. D. Wang, N. Liu, J. Zhang, X. Zhao, W. Zhang and M. Zhang, *Journal of*

RSC Advances Accepted Manuscript

Molecular Catalysis A: Chemical, 2014, **393**, 47-55.

20. B. Li, W. Ma, J. Liu, C. Han, S. Zuo and X. Li, *Catalysis Communications*, 2011, **13**, 101-105.

21. J.-T. Sun, C.-Y. Hong and C.-Y. Pan, *The Journal of Physical Chemistry C*, 2010, **114**, 12481-12486.

22. K. S. Sing, *Pure and applied chemistry*, 1985, **57**, 603-619.

23. Y. T. Joo, K. H. Jung, M. J. Kim and Y. Kim, *Journal of Applied Polymer Science*, 2013, **127**, 1508-1518.

24. G. M. El Shafei and M. Mokhtar, *Colloids and Surfaces A: Physicochemical and Engineering Aspects*, 1995, **94**, 267-277.

25. S. R. Seyedmonir, S. Abdo and R. F. Howe, *The Journal of Physical Chemistry*, 1982, **86**, 1233-1235.

26. D. Zhao, Y. Wang, E. Duan and J. Zhang, *Fuel Processing Technology*, 2010, **91**, 1803-1806.

27. G. Zhu, W. Zhu, H. Li, W. Huang, Y. Jiang, Y. Ding and W. Jiang, *Petroleum Science and Technology*, 2012, **30**, 2407-2416.

28. Y. K. Park, S. Y. Kim, H. J. Kim, K. Y. Jung, K.-E. Jeong, S.-Y. Jeong and J.-K. Jeon, *Korean Journal of Chemical Engineering*, 2010, **27**, 459-464.

29. D. Liu, J. Gui, Y.-K. Park, S. Yang, Y. Gao, X. Peng and Z. Sun, *Korean Journal of Chemical Engineering*, 2012, **29**, 49-53.

30. S. Otsuki, T. Nonaka, N. Takashima, W. Qian, A. Ishihara, T. Imai and T. Kabe, *Energy & Fuels*, 2000, **14**, 1232-1239.

RSC Advances Accepted Manuscript

31. J. Ge, Y. Zhou, Y. Yang and M. Xue, *Industrial & Engineering Chemistry Research*, 2011, **50**, 13686-13692.

32. A. Sengupta, P. D. Kamble, J. K. Basu and S. Sengupta, *Industrial & Engineering Chemistry Research*, 2011, **51**, 147-157.

33. J. Qiu, G. Wang, D. Zeng, Y. Tang, M. Wang and Y. Li, *Fuel Processing Technology*, 2009, **90**, 1538-1542.

RSC Advances Accepted Manuscript

Table 1. Physical Properties of the $H_4SiMo_{12}O_{40}@SiO_2$-X (X= 10, 20, 30, and 40) Hollow Sphere

Catalyst	Surface area (m^2/g)[a]	Pore volume(cm^3/g)[b]	Pore size (nm)[c]
$SiMo@SiO_2$-10	802	0.46	2.3
$SiMo@SiO_2$-20	713	0.41	2.5
$SiMo@SiO_2$-30	653	0.39	2.7
$SiMo@SiO_2$-40	440	0.32	2.9

a Calculated by the BET equation.

b BJH desorption pore volume.

c BJH desorption average pore size.

RSC Advances Accepted Manuscript

Figure captions

Fig.1. Core-shell structure of the synthesized $H_4SiMo_{12}O_{40}@SiO_2$.

Fig.2. (a) TEM images of MoO_2 nanoparticles (200 nm), (b) size distribution of MoO_2 nanoparticles (200 nm), (c–f) TEM images of MoO_2 nanoparticles (2 nm), $MoO_2@SiO_2$, $Mo^{VI}@SiO_2$, and $H_4SiMo_{12}O_{40}@SiO_2$.

Fig. 3. (a) XRD patterns of (a) $H_4SiMo_{12}O_{40}@SiO_2$-10, (b) $H_4SiMo_{12}O_{40}@SiO_2$-20, (c) $H_4SiMo_{12}O_{40}@SiO_2$-30, and (d) $H_4SiMo_{12}O_{40}@SiO_2$-40. (b) XRD patterns of MoO_2 nanoparticles.

Fig. 4. (a) Nitrogen adsorption/desorption isotherms of (a) $H_4SiMo_{12}O_{40}@SiO_2$-10, (b) $H_4SiMo_{12}O_{40}@SiO_2$-20, (c) $H_4SiMo_{12}O_{40}@SiO_2$-30, and (d) $H_4SiMo_{12}O_{40}@SiO_2$-40. (b) Pore size distribution curve of $H_4SiMo_{12}O_{40}@SiO_2$-20

Fig. 5. FT-IR spectra of (a) $H_4SiMo_{12}O_{40}@SiO_2$-10, (b) $H_4SiMo_{12}O_{40}@SiO_2$-20, (c) $H_4SiMo_{12}O_{40}@SiO_2$-30, and (d) $H_4SiMo_{12}O_{40}@SiO_2$-40.

Fig. 6. Effect of (a) O/S molar ratio, (b) catalyst dosage, and (c) reaction temperature on the sulfur removal of DBT. Experimental conditions: T=333 K, O/S=12, catalyst dosage=0.1 g/10 mL, t=2.5 h.

Fig. 7. Removal of S-compounds versus reaction time. Experimental conditions: T=333 K, O/S=12, catalyst dosage=0.1 g/10 mL.

Fig. 8. (a) Pseudo-first-order rate model data at different temperatures. (b) Determination of activation energy for the reaction.

Fig. 9. Effect of recycling times on DBT conversion. Experimental conditions: T=333 K, O/S=12, catalyst dosage=0.1 g/10 mL, t=2.5 h.

RSC Advances Accepted Manuscript

Fig. 10. FT-IR spectra of (a) $H_4SiMo_{12}O_{40}$@SiO_2-20, (b) After recovery of $H_4SiMo_{12}O_{40}$@SiO_2-20,

RSC Advances Accepted Manuscript

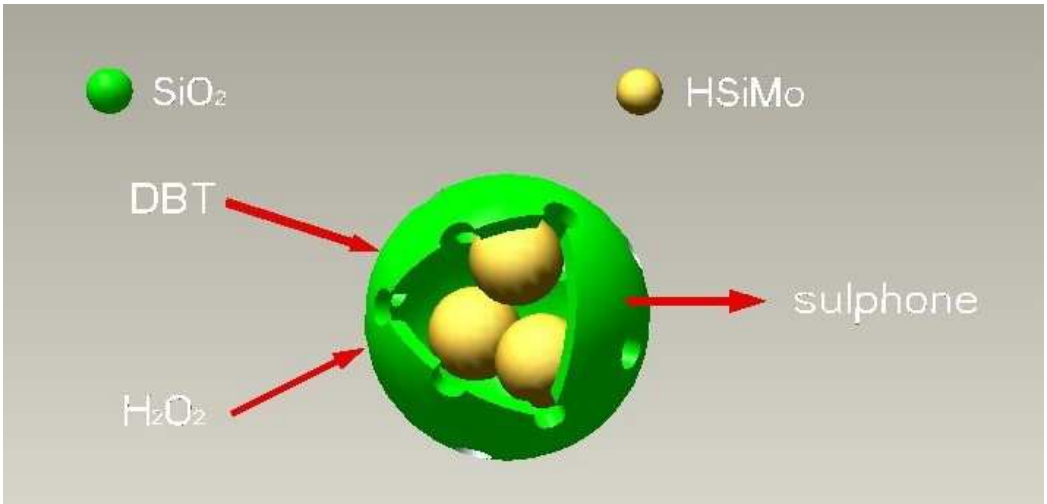

Fig.1. Core-shell structure of the synthesized $H_4SiMo_{12}O_{40}@SiO_2$.

RSC Advances Accepted Manuscript

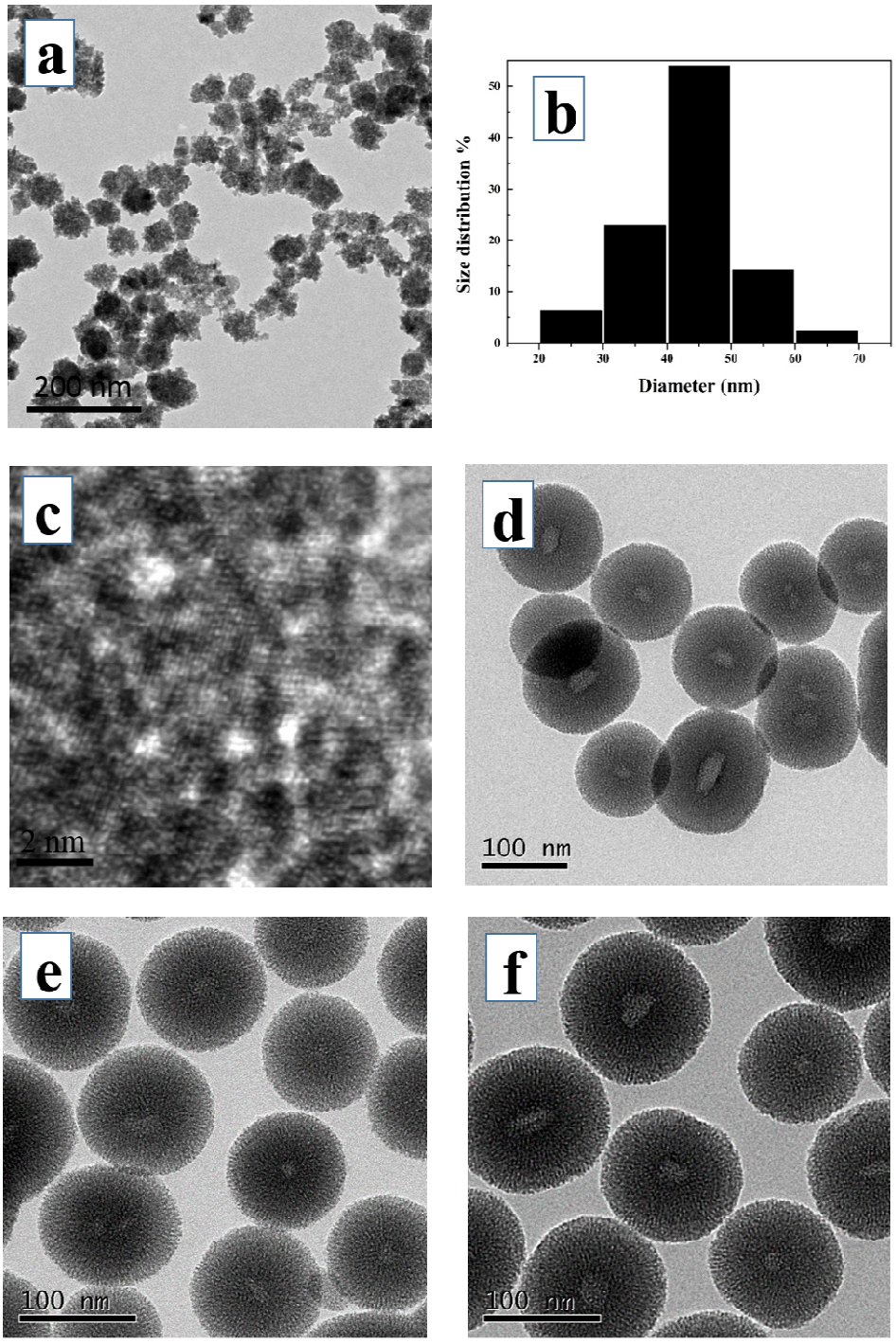

Fig.2. (a) TEM images of MoO_2 nanoparticles, (b) size distribution of MoO_2 nanoparticles, (c–f) TEM images of MoO_2 nanoparticles (2 nm), MoO_2@SiO_2, Mo^{VI}@SiO_2, and $H_4SiMo_{12}O_{40}$@SiO_2.

RSC Advances Accepted Manuscript

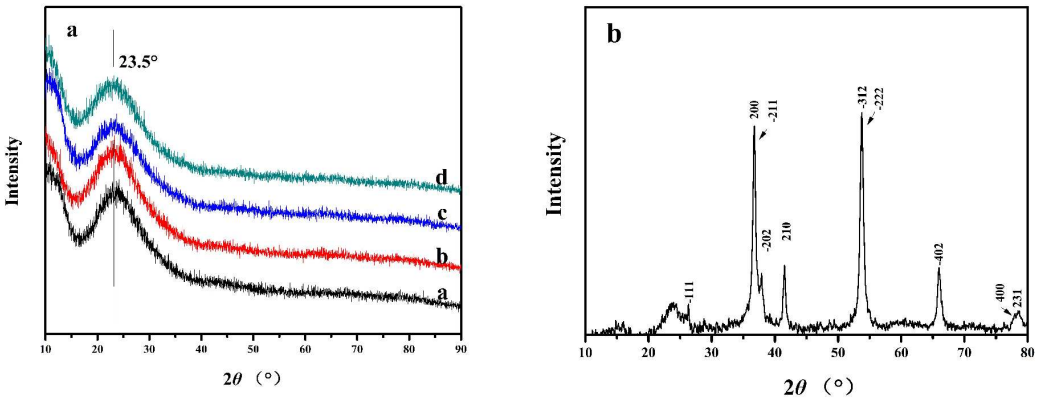

Fig. 3. (a) XRD patterns of (a) $H_4SiMo_{12}O_{40}$@SiO_2-10, (b) $H_4SiMo_{12}O_{40}$@SiO_2-20, (c) $H_4SiMo_{12}O_{40}$@SiO_2-30, and (d) $H_4SiMo_{12}O_{40}$@SiO_2-40. (b) XRD patterns of MoO_2 nanoparticles.

RSC Advances Accepted Manuscript

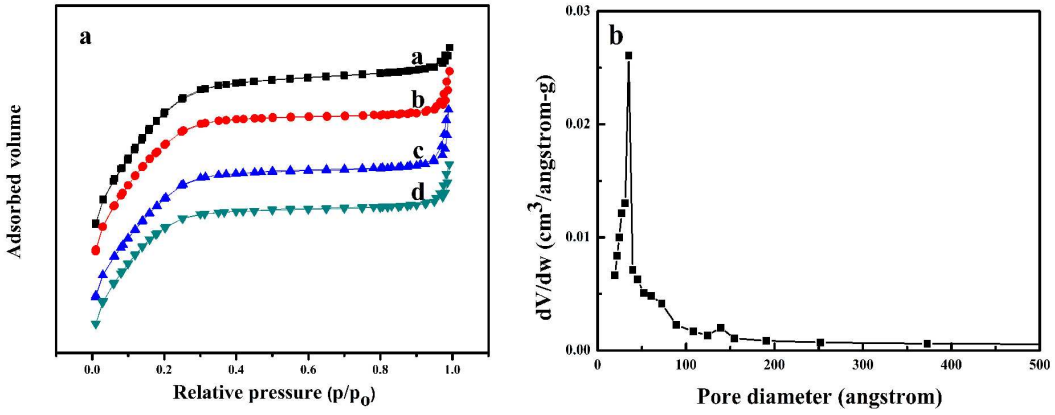

Fig. 4. (a) Nitrogen adsorption/desorption isotherms of (a) $H_4SiMo_{12}O_{40}$@SiO_2-10, (b) $H_4SiMo_{12}O_{40}$@SiO_2-20, (c) $H_4SiMo_{12}O_{40}$@SiO_2-30, and (d) $H_4SiMo_{12}O_{40}$@SiO_2-40. (b) Pore size distribution curve of $H_4SiMo_{12}O_{40}$@SiO_2-20

RSC Advances Accepted Manuscript

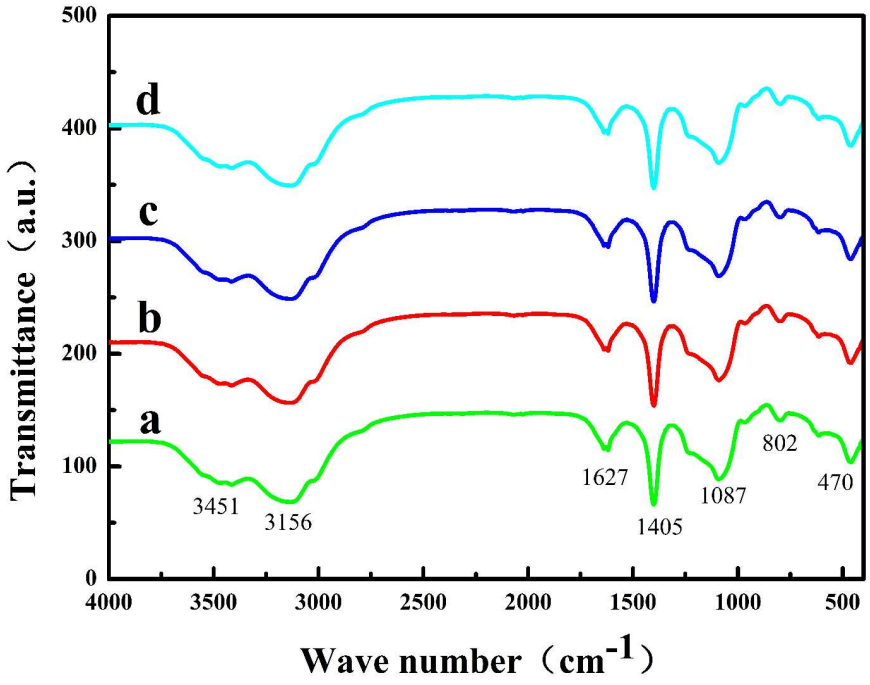

Fig. 5. FT-IR spectra of (a) $H_4SiMo_{12}O_{40}$@SiO_2-10, (b) $H_4SiMo_{12}O_{40}$@SiO_2-20, (c) $H_4SiMo_{12}O_{40}$@SiO_2-30, and (d) $H_4SiMo_{12}O_{40}$@SiO_2-40.

RSC Advances Accepted Manuscript

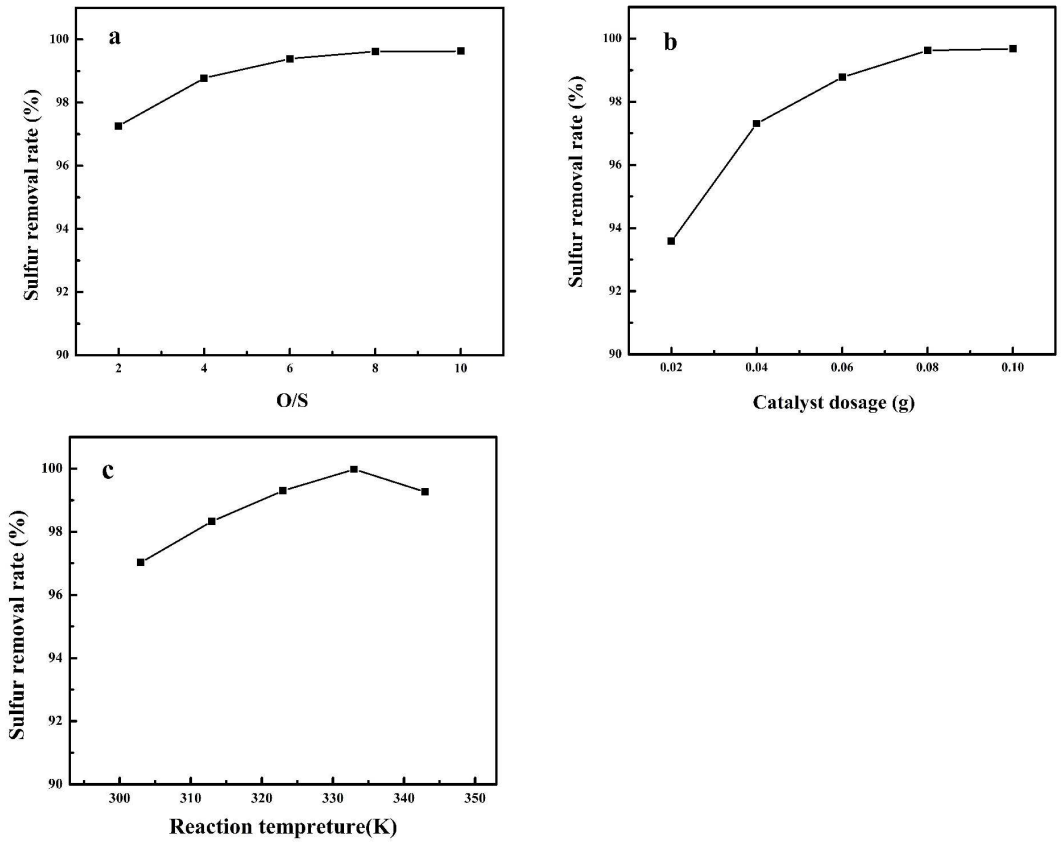

Fig. 6. Effect of (a) O/S molar ratio, (b) catalyst dosage, and (c) reaction temperature on the sulfur removal of DBT. Experimental conditions: T=333 K, O/S=12, catalyst dosage=0.1 g/10 mL, t=2.5 h.

RSC Advances Accepted Manuscript

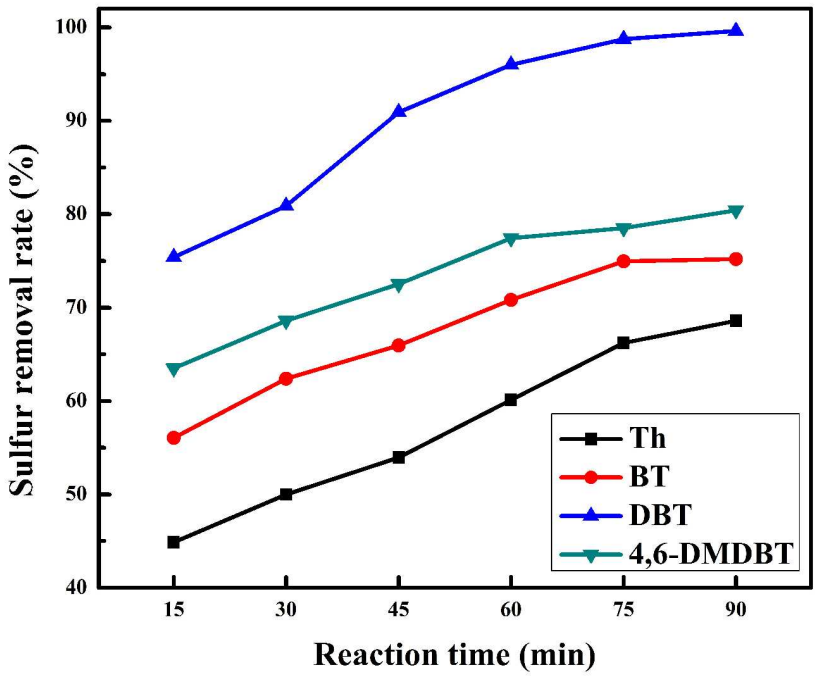

Fig. 7. Removal of S-compounds versus reaction time. Experimental conditions: T=333 K, O/S=12, catalyst dosage=0.1 g/10 mL.

RSC Advances Accepted Manuscript

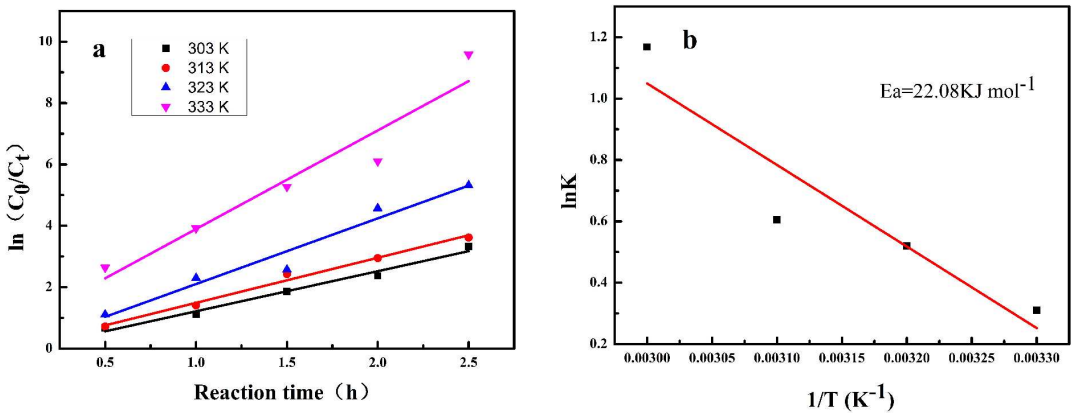

Fig. 8. (a) Pseudo-first-order rate model data at different temperatures. (b) Determination of activation energy for the reaction.

RSC Advances Accepted Manuscript

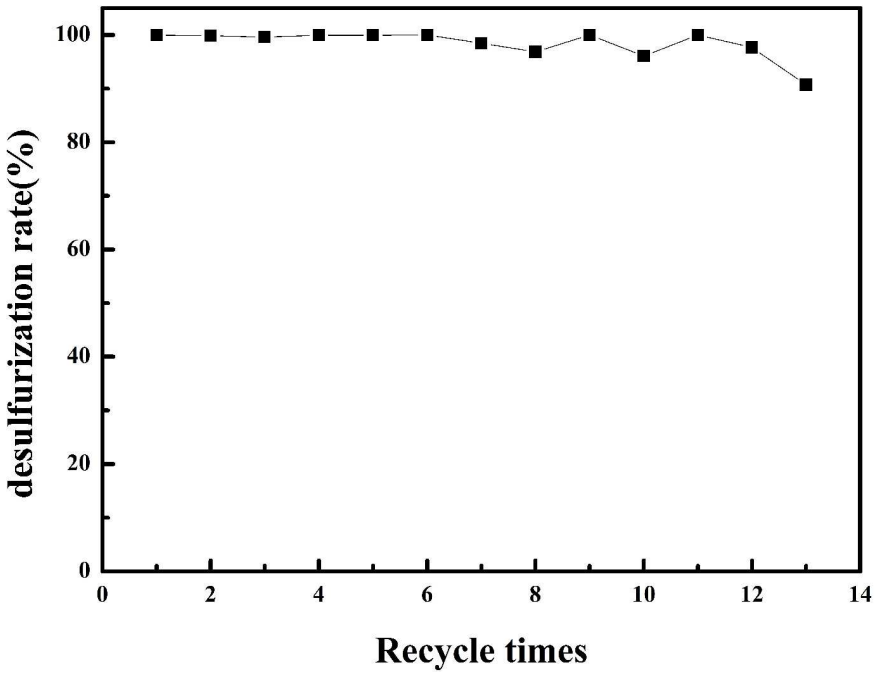

Fig. 9. Effect of recycling times on DBT conversion. Experimental conditions: T=333 K, O/S=12, catalyst dosage=0.1 g/10 mL, t=2.5 h.

RSC Advances Accepted Manuscript

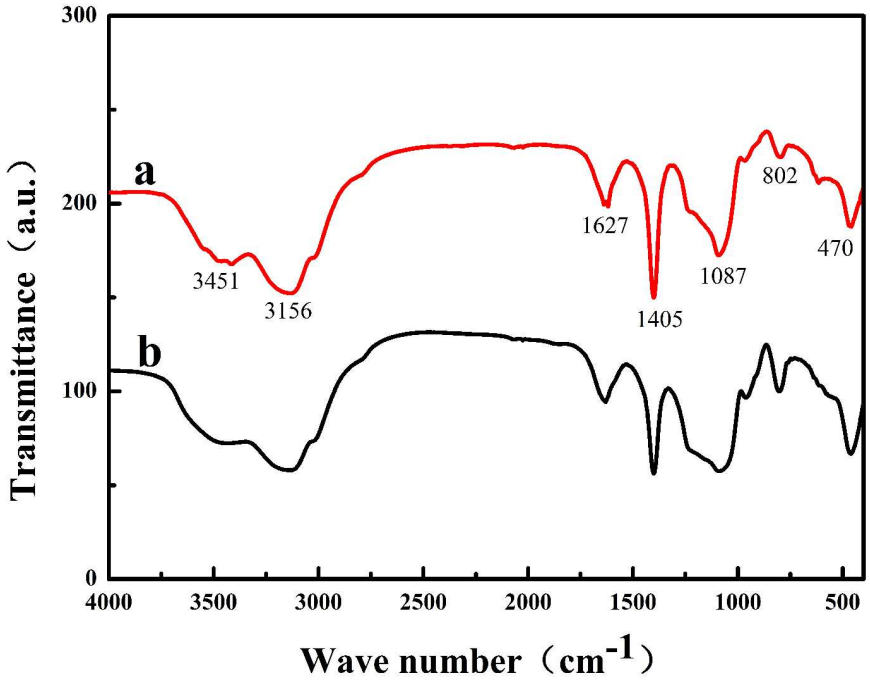

Fig. 10. FT-IR spectra of (a) $H_4SiMo_{12}O_{40}$@SiO_2-20, (b) After recovery of $H_4SiMo_{12}O_{40}$@SiO_2-20,

RSC Advances Accepted Manuscript